MITSUBISHI ELECTRIC RESEARCH LABORATORIES
http://www.merl.com

Proportional-Integral Extremum Seeking for Vapor Compression Systems

Burns, D.J.; Laughman, C.R.; Guay, M.

TR2019-032 June 22, 2019

Abstract

In this paper, we optimize vapor compression system power consumption through the application of a novel proportional–integral extremum seeking controller (PI-ESC) that converges at the same timescale as the process. This extremum seeking method uses time-varying parameter estimation to determine the local gradient in the map from manipulated inputs to performance output. Additionally, the extremum seeking control law includes terms proportional to the estimated gradient, which requires subsequent modification of the estimation routine in order to avoid bias. The PI-ESC algorithm is derived and compared to other methods on a benchmark example that demonstrates the improved convergence rate of PI-ESC. PI-ESC is applied to the problem of compressor discharge temperature setpoint selection for a vapor compression system such that power consumption is driven to a minimum. A physicsbased simulation model of the vapor compression system is used to demonstrate that with PI-ESC, convergence to the optimal operating point occurs faster than the bandwidth of typical disturbances—enabling application of extremum seeking control to vapor compression systems in environments under realistic operating conditions. Finally, experiments on a production room air conditioner installed in an adiabatic test facility validate the approach in the presence of significant noise and actuator and sensor quantization.

IEEE Transactions on Control Systems Technology

Proportional–Integral Extremum Seeking for Vapor Compression Systems

Daniel J. Burns,† *Senior Member, IEEE*, Christopher R. Laughman, *Member, IEEE* and Martin Guay, *Senior Member, IEEE*

***Abstract*—In this paper, we optimize vapor compression system power consumption through the application of a novel proportional–integral extremum seeking controller (PI-ESC) that converges at the same timescale as the process. This extremum seeking method uses time-varying parameter estimation to determine the local gradient in the map from manipulated inputs to performance output. Additionally, the extremum seeking control law includes terms proportional to the estimated gradient, which requires subsequent modification of the estimation routine in order to avoid bias. The PI-ESC algorithm is derived and compared to other methods on a benchmark example that demonstrates the improved convergence rate of PI-ESC.**

PI-ESC is applied to the problem of compressor discharge temperature setpoint selection for a vapor compression system such that power consumption is driven to a minimum. A physics-based simulation model of the vapor compression system is used to demonstrate that with PI-ESC, convergence to the optimal operating point occurs faster than the bandwidth of typical disturbances—enabling application of extremum seeking control to vapor compression systems in environments under realistic operating conditions. Finally, experiments on a production room air conditioner installed in an adiabatic test facility validate the approach in the presence of significant noise and actuator and sensor quantization.

I. Introduction

VAPOR compression machines move thermal energy from a low temperature zone to a high temperature zone, performing either cooling or heating depending on the configuration of the refrigerant piping. The relative simplicity of the machine and its effective and robust performance has enabled the vapor compression machine in various forms and packages to become widely deployed, and it is critical to modern comfort standards and the global food production and distribution industries. It is the most common means for commercial and residential space cooling [1], often employed for space or water heating [2], and extensively used in refrigeration (both stationary and mobile [3]), desalination [4], and cryogenic applications [5].

In many control formulations for vapor compression machines the evaporator superheat temperature is selected as a regulated variable for cycle efficiency and equipment protection [6], [7], [8]. However, a measurement of the evaporator superheat is often not available on production equipment. Instead, cycle efficiency can be maintained through the regulation of the compressor discharge temperature to a setpoint that depends on the heat load and the outdoor air temperature disturbances. The discharge temperature is often measured for equipment protection making it a commonly available signal, and because the refrigerant state at this location in the cycle is always superheated, this signal is a one-to-one function of the disturbances over the full range of expected operating points [9]. Because discharge temperature changes with heat loads and outdoor air temperatures, its setpoint cannot be regulated to a constant, but instead must vary with external conditions. It is the aim of this paper to automate the generation of such setpoints.

However, determining these energy-optimal setpoints is not straightforward. Models of the vapor compression system that attempt to describe the influence of commanded inputs on thermodynamic behavior and power consumption are often low in fidelity, and while they may have useful predictive capabilities near the conditions at which they were calibrated, the environments into which these systems are deployed are so diverse as to render comprehensive calibration and model tuning intractable. Therefore, relying on model-based strategies for realtime optimization is problematic.

Recently, model-free extremum seeking methods that operate in realtime and aim to optimize a cost have received increased attention and have demonstrated improvements in the optimization of vapor compression systems and other HVAC applications [10], [11], [12], [13], [14]. To date, the dominant extremum seeking algorithm that appears in the HVAC research literature is the traditional perturbation-based algorithm first developed in the 1920s [15] and re-popularized in the late 1990s by an elegant proof of convergence for a general class of nonlinear systems [16].

Most extremum seeking controllers can be viewed as a gradient descent optimization algorithm implemented as a feedback controller [17] and therefore consists of two main components: (1) an estimation part that determines the local gradient of the performance map with respect to the decision variables, and (2) a control law part that manipulates the decision variables to steer the system to the optimizer of the map. In the traditional perturbation-based method, a sinusoidal term is added to the input at a slower frequency than the natural plant dynamics, inducing a sinusoidal response in the performance metric and introducing a timescale slower than the process dynamics. The controller then filters this signal to obtain an estimate of the gradient. Averaging the perturbation introduces yet another (and slower) time scale in the opti-

D. J. Burns (burns@merl.com) and C. R. Laughman (laughman@merl.com) are with Mitsubishi Electric Research Laboratories, 201 Broadway, Cambridge, MA 02139.

M. Guay is with the Department of Chemical Engineering, Queen's University, Kingston, ON, Canada. email: martin.guay@chee.queensu.ca

† Corresponding author.

mization process. Using a gradient estimate obtained in this way, the control law integrates the estimated gradient to drive the gradient to zero. As a result, the traditional perturbation-based extremum seeking converges to the neighborhood of the optimum at about two timescales slower than the plant dynamics due to inefficient estimation of the gradient, and slow (integral-action dominated) adaptation in the control law. For thermal systems such as vapor compression machines where the dynamics are already on the order of tens of minutes, the slow convergence property of perturbation-based extremum seeking becomes an impediment to wide-scale deployment.

However, convergence rates can be improved by addressing both components of the extremum seeking algorithm. An efficient method for estimating gradients is developed that treats the gradient as an unknown time-varying parameter to be identified. Time-varying extremum seeking (TV-ESC) uses adaptive filtering techniques to estimate the parameters of the gradient—eliminating the timescale associated with averaging perturbations [18]. However, that method does not modify the control law, and while convergence is significantly improved compared to the perturbation-based method, the control law of TV-ESC remains integral-action dominated. In this paper, we apply PI-ESC [19] to vapor compression systems in which the algorithm estimates the gradient using the efficient time-varying approach, but also modifies the control law to include a term proportional to the value of the estimated gradient. This term drives the system toward the optimum operating point at the same timescale as the vapor compression system dynamics.

The remainder of this paper is organized as follows: The vapor compression system and control objectives are described in Section II. The discrete-time PI-ESC algorithm is then derived in Section III and its convergence properties are demonstrated in comparison to other ESC methods. Section IV presents simulated and experimental results and concluding remarks are offered in Section V.

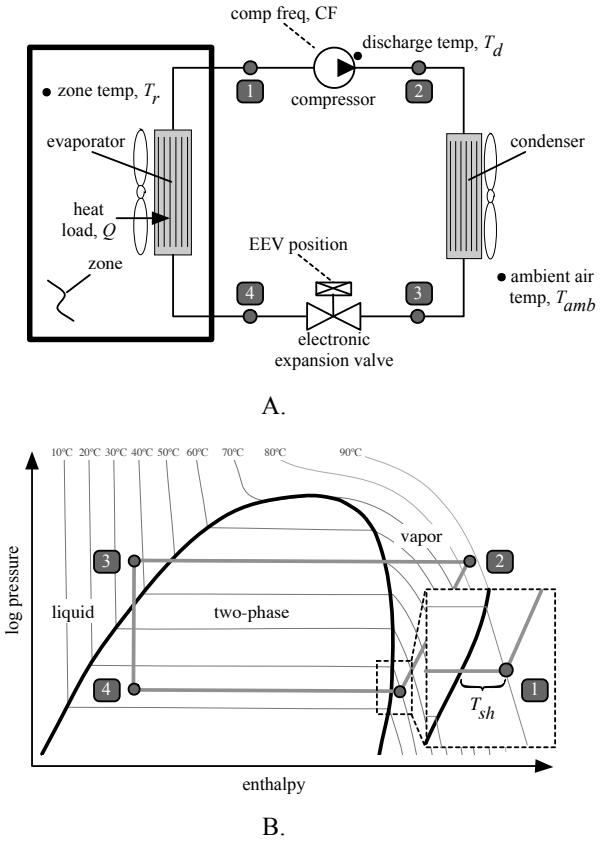

Fig. 1. A. Principal components of the vapor compression cycle. B. Idealized refrigeration cycle shown in pressure–enthalpy coordinates. Inset: Visualization of evaporator superheat temperature.

II. Vapor Compression System

This section briefly describes the operation of the vapor compression system (VCS) and control inputs, measurements and objectives. The specific application considered in this paper employs the VCS as an air conditioner, and therefore certain assumptions on heat exchanger type, refrigerant flow direction and control objectives have been made, although other applications of VCS (refrigeration, heat pumps, etc.) can be considered with straightforward substitutions of machine configurations.

A. Physical Description

The arrangement of the four principal components of the VCS are shown in Fig. 1A, and the refrigerant state between those components are shown on an idealized pressure–enthalpy cycle diagram in Fig. 1B. Starting from the point labeled '1,' low pressure refrigerant in the vapor state enters the compressor suction port. The compressor performs work on the refrigerant to increase the pressure and temperature, and the amount of work is controlled by the compressor rotational frequency CF. A sensor measures the refrigerant discharge temperature T_d exiting the compressor. High temperature and pressure refrigerant (point '2') is then routed to a heat exchanger across which a fan forces air. Heat is removed from the refrigerant and rejected to the surrounding air, which is at a temperature measured by an ambient sensor, T_{amb}. The ambient temperature is considered a measured disturbance. As the specific enthalpy of the refrigerant is reduced inside the heat exchanger, it condenses and ultimately exits as a high pressure liquid (point '3'). The refrigerant then flows through an electronic expansion valve which simultaneously reduces the pressure and temperature in an isenthalpic process. The electronic expansion valve position (EEV) controls the size of the valve orifice. The low pressure, low temperature refrigerant exiting the valve (point '4') is a two-phase mixture of liquid and vapor and is passed to another heat exchanger. Again, a fan forces air across the heat exchanger. Heat is absorbed by the refrigerant from the air in the zone to be conditioned, which is at a temperature measured by a zone temperature sensor, T_r. As the specific enthalpy of the refrigerant increases, it evaporates and exits the heat exchanger as a low pressure vapor. The refrigerant is routed to the compressor inlet, completing the cycle. Finally, a heat load is assumed in the zone and is an unmeasured disturbance. If the heat load balances the heat removed by the evaporator, the zone temperature does not change, otherwise the zone temperature will increase or decrease when the heat load is greater or less than the energy

removed by the evaporator.

Remark 1: Note the lines of constant temperature in Fig. 1B. The evaporating and condensing processes of refrigerant phase change occurs at a constant temperature (within the 'two-phase' region between the saturation curves of Fig. 1B) when the refrigerant used is a pure or near-azeotropic fluid [20], as is the case for many commercially-available systems. Therefore, the thermodynamic state of refrigerant undergoing a phase change process is not measurable from temperature or pressure sensors.

B. Evaporator Superheat vs. Discharge Temperature

Consider again the refrigerant in the evaporator. As heat is absorbed, the state changes from a mostly liquid two-phase mixture to a mostly vapor mixture, ultimately reaching a saturated vapor state during an isothermal process. As further heat is absorbed by a saturated vapor, a measurable change in temperature occurs. This increase in temperature above the saturation temperature is called the superheat temperature T_{sh},

$$T_{sh} = T_1 - T_{\text{sat},\, p_1}, \tag{1}$$

where T_1 is the temperature of the refrigerant at point '1' on Fig. 1B, and $T_{\text{sat},\, p_1}$ is the saturation temperature of the refrigerant at that pressure p_1. Note that superheat temperature is not defined for values less than zero (see Remark above.)

Many control designs use T_{sh} as a process variable and regulate it to a small positive value using the EEV. A low superheat temperature ensures that the majority of the evaporator contains two-phase refrigerant, which has a much higher heat transfer coefficient than refrigerant in the vapor state, and therefore low T_{sh} is associated with good cycle efficiency. However, disturbances can perturb the superheat temperature to zero, causing the feedback loop to open. As a result, many T_{sh} controllers have low gain in order to tolerate occasional open loop operation, and this leads to the well-known issue of valve 'hunting,' which is limit cycling induced by low gain feedback [21], whether that feedback is mechanical as for thermostatic expansion valves or electronic as for EEVs. In contrast to previous work, we select the compressor discharge temperature T_d as a process variable. As seen from point '2' of Fig. 1B, the refrigerant at the compressor outlet is far from the saturation boundary and within the measurable superheated region where temperatures at this point in the cycle are a one-to-one function of the disturbances, which maintains system observability and enables higher gain feedback.

However, while controlling T_d has certain advantages, it cannot be regulated to a constant, but instead must be scheduled on system disturbances. In following sections, we use extremum seeking to determine setpoints for a T_d regulator.

C. Controller Architecture

The control objective is to regulate the zone temperature T_r to a setpoint determined by an occupant, rejecting heat load Q and ambient air temperature T_{amb} disturbances. Further, power consumption P must be minimized at steady state. The system actuators are the compressor frequency CF, and electronic expansion valve position EEV. We assume that the fan speeds are not manipulated by the controller. The zone temperature T_r, discharge temperature T_d, and system power consumption P are measured.

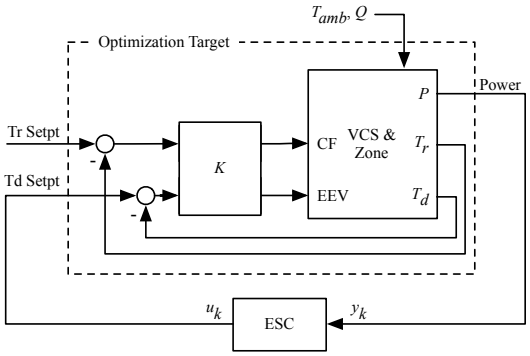

Fig. 2. Actuator commands are computed by the feedback regulator, which drives the the vapor compression system toward setpoints that consist of external setpoints (*e.g.*, a desired zone temperature setpoint) and machine setpoints (*e.g.*, a compressor discharge temperature setpoint). The PI-ESC selects discharge temperature setpoints u_k that minimize the system power consumption y_k in the presence of disturbances such as changes in outdoor air temperature and heat load.

The control architecture is shown in Fig. 2. A multivariable feedback controller K is designed to drive the room temperature error and the discharge temperature error to zero. A relative gain array (RGA) analysis has shown good decoupling is achieved by pairing T_r regulation with CF, and T_d tracking with the EEV, and therefore we begin with K as two decentralized PI controllers. However, we introduce coupling in the controller K as follows: the output of the CF PI controller (suitably scaled and filtered) is provided as an input to the EEV PI controller. This coupling has been shown to dramatically improve disturbance rejection when the compressor frequency is a control input and the compressor discharge temperature is a controlled output [22].

The T_r setpoint is assumed to originate from an exogenous source (*i.e.,* a thermostat). The T_d setpoint is determined from an extremum seeking controller (ESC) configured to obtain the discharge temperature that minimizes power consumption. Sensor information is quantized in roughly 0.5 C increments. Permissible compressor frequency commands in Hz are quantized to integer values, with some additional ranges excluded to avoid mechanical resonances and detrimental electrical interactions between the power inverters and the supply mains. Finally, because the system power consumption is strongly dependent on CF, power measurements also attain discrete values.

III. Proportional–Integral Extremum Seeking Controller

This section outlines the development of an extremum seeking controller based on a time-varying estimate of the gradient of the cost and a PI control law to drive the system to its optimum operating point. See [19] for the full development and stability and convergence analysis in discrete time.

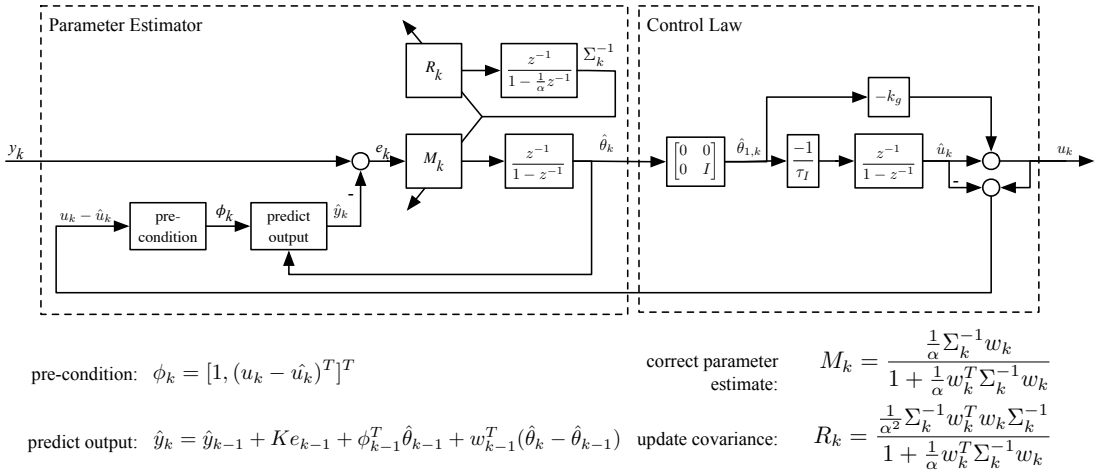

Fig. 3. Overview of the PI-ESC algorithm.

A. PI-ESC Development

We consider a class of nonlinear systems of the form:

$$\begin{aligned} x_{k+1} &= x_k + f(x_k) + g(x_k)u_k \quad (2)\\ y_k &= h(x_k) \quad (3)\end{aligned}$$

where $x_k \in \mathbb{R}^n$ is the vector of state variables at time k, u_k is the input variable at time k taking values in $\mathscr{U} \subset \mathbb{R}$ and $y_k \in \mathbb{R}$ is the objective function at step k, to be minimized. It is assumed that $f(x_k)$ and $g(x_k)$ are smooth vector valued functions and that $h(x_k)$ is a smooth function.

We assume that the cost $h(x)$ is relative order one and satisfies the optimality conditions:

1) $\frac{\partial h(x^*)}{\partial x} = 0$
2) $\frac{\partial^2 h(x)}{\partial x \partial x^T} > \beta I$, $\forall x \in \mathbb{R}^n$

where β is a strictly positive constant.

We let $\alpha(x_k, \hat{u}_k) = x_k + f(x_k) + g(x_k)\hat{u}_k$. The rate of change of the cost function $y_k = h(x_k)$ is given by:

$$\begin{aligned} h(x_{k+1}) - h(x_k) =& h(x_k + f(x_k) + g(x_k)u_k) \\ & - h(\alpha(x_k, \hat{u}_k)) + h(\alpha(x_k, \hat{u}_k)) - h(x_k).\end{aligned}$$

Using a second order Taylor expansion on the first two terms we can rewrite the cost dynamics as:

$$y_{k+1} - y_k = \Psi_{0,k}(x_k, \hat{u}_k) + \Psi_{1,k}(x_k, u_k, \hat{u}_k)(u_k - \hat{u}_k).$$

where $\Psi_{0,k}(x_k, \hat{u}_k) = h(\alpha(x_k, \hat{u}_k)) - h(x_k)$, and $\Psi_{1,k}(x_k, u_k, \hat{u}_k) = (\nabla h(\alpha(x_k, \hat{u}_k)) g(x_k) + \frac{1}{2}(u_k - \hat{u}_k)^\top g(x_k)^\top \nabla^2 h(\tilde{y}_k) g(x_k)$ where $\tilde{y}_k = \alpha(x_k, \hat{u}_k) + c g(x_k)(u_k - \hat{u}_k)$ for $c \in (0,1)$. By the relative order one assumption on $h(x)$, the system's dynamics can be decomposed and written as:

$$\begin{aligned} \xi_{k+1} &= \xi_k + \psi(\xi_k, y_k) \quad (4)\\ y_{k+1} &= y_k + \Psi_{0,k}(x_k, \hat{u}_k) + \Psi_{1,k}(x_k, u_k, \hat{u}_k)(u_k - \hat{u}_k) \quad (5)\end{aligned}$$

where $\xi_k \in \mathbb{R}^{n-1}$ and $\psi(\xi_k, y_k)$ is a smooth vector valued function. Based on Equation (5), the cost function dynamics is parameterized as follows:

$$y_{k+1} = y_k + \theta_{0,k} + \theta_{1,k}(u_k - \hat{u}_k)$$

where the time-varying parameters $\theta_{0,k}$ and $\theta_{1,k}$ represent $\Psi_{0,k}$ and $\Psi_{1,k}$, and are to be identified. It is important to note that the unbiased correct estimation of $\theta_{1,k}$ requires the estimation of the drift parameter $\theta_{0,k}$.

Let $\hat{\theta}_{0,k}$ and $\hat{\theta}_{1,k}$ denote the estimates of $\theta_{0,k}$ and $\theta_{1,k}$, respectively, and consider the following state predictor

$$\begin{aligned} \hat{y}_{k+1} &= \hat{y}_k + \hat{\theta}_{0,k} + \hat{\theta}_{1,k}(u_k - \hat{u}_k) \\ &+ K_k e_k - w_{k+1}(\hat{\theta}_k - \hat{\theta}_{k+1}) \quad (6)\end{aligned}$$

where $\hat{\theta}_k = [\hat{\theta}_{0,k}, \hat{\theta}_{1,k}^T]^T$ is the vector of parameter estimates at time step k given by any update law, K_k is a correction factor at time step k, $e_k = y_k - \hat{y}_k$ is the state estimation error. We let $\phi_k = [1, (u_k - \hat{u}_k)^T]^T$ and we denote the parameter estimation error at step k by $\tilde{\theta}_k = \theta_k - \hat{\theta}_k$. The variable w_k is the following output filter at time step k

$$w_{k+1} = w_k + \phi_k - K_k w_k, \quad (7)$$

with $w_0 = 0$. Using the state predictor defined in (6) and the output filter defined in (7), the prediction error $e_k = y_k - \hat{y}_k$ is given by

$$\begin{aligned} e_{k+1} &= e_k + \phi_k \tilde{\theta}_{k+1} - K_k e_k \\ &+ w_{k+1}(\hat{\theta}_k - \hat{\theta}_{k+1}) + w_{k+1}(\theta_{k+1} - \theta_k) \\ e_0 &= y_0 - \hat{y}_0. \quad (8)\end{aligned}$$

An auxiliary variable η_k is introduced which is defined as $\eta_k = e_k - w_k^T \tilde{\theta}_k$. Its dynamics are given by

$$\begin{aligned} \eta_{k+1} &= e_{k+1} - w_{k+1}\tilde{\theta}_{k+1} \\ \eta_0 &= e_0. \quad (9)\end{aligned}$$

Since the rate of change of the parameter vector, $\theta_{k+1} - \theta_k$, is unknown, the auxiliary variable η_k is unknown. Therefore, it is necessary to use an estimate, $\hat{\eta}$, of η. The estimate is generated by the recursion:

$$\hat{\eta}_{k+1} = \hat{\eta}_k - K_k \hat{\eta}_k \quad (10)$$

Let the identifier matrix Σ_k be defined as

$$\Sigma_{k+1} = \alpha \Sigma_k + w_k^T w_k, \quad \Sigma_0 = \alpha I \succ 0 \quad (11)$$

with an inverse generated by the recursion

$$\Sigma_{k+1}^{-1} = \Sigma_k^{-1} + \left(\frac{1}{\alpha} - 1\right)\Sigma_k^{-1} - \frac{1}{\alpha^2}\Sigma_k^{-1} w_k \left(1 + \frac{1}{\alpha} w_k^T \Sigma_k^{-1} w_k\right)^{-1} w_k^T \Sigma_k^{-1} \quad (12)$$

Using (6), (7), and (10), the parameter update law is

$$\hat{\theta}_{k+1} = \hat{\theta}_k + \frac{1}{\alpha}\Sigma_k^{-1} w_k^T \left(I + \frac{1}{\alpha} w_k \Sigma_k^{-1} w_k^T\right)^{-1} (e_k - \hat{\eta}_k) \quad (13)$$

In order to prevent any peaking arising from the estimation, the parameter estimate are constrained to remain inside compact convex set in the parameter space denoted by Θ. Consequently, the true value, θ_k, is assumed to be contained inside Θ. To ensure that the parameter estimates remain within the constraint set Θ, we use a projection operator [18], [23]

$$\bar{\hat{\theta}}_{k+1} = \text{Proj}\{\hat{\theta}_k + \Sigma_k^{-1} w_k^T \left(I + w_k \Sigma_k^{-1} w_k^T\right)^{-1} (e_k - \hat{\eta}_k), \Theta\} \quad (14)$$

which completes the parameter estimation component of the controller.

Finally, the proposed control law is given by:

$$u_k = -k_g \hat{\theta}_{1,k} + \hat{u}_k \quad (15)$$

$$\hat{u}_{k+1} = \hat{u}_k - \frac{1}{\tau_I}\hat{\theta}_{1,k}. \quad (16)$$

where k_g and τ_I are positive constants to be assigned.

B. PI-ESC Summary

The final PI-ESC algorithm consists of a time varying parameter estimation routine for determining $\hat{\theta}_{0,k}$ and $\hat{\theta}_{1,k}$ and consists of Equations (6), (7), (10), (12), and (14) with tuning parameters K and α. The control law is given by Equations (15) and (16) and contains terms proportional to the estimated gradient and with integral action necessary to identify optimal equilibrium conditions, and is tuned using the parameters k_g and τ_I. A block diagram of the PI-ESC algorithm summarizing the main signal flow is shown in Figure 3. Guidance for tuning the parameters of these equations can be found in [19].

Note that the PI-ESC algorithm does not require averaging the effect of the perturbation as with traditional perturbation-based extremum seeking. For this reason, proportional-integral extremum seeking converges substantially faster, as demonstrated in the following comparison.

C. Comparison of extremum seeking methods

This section discusses the convergence performance of three extremum seeking controllers applied to a previously published example problem [9]. Traditional perturbation-based extremum seeking control [24], time-varying extremum seeking control [18] and proportional–integral extremum seeking control [19] are each applied to the problem of finding input values to a simple Hammerstein system that minimize its output, where the controllers have no knowledge of the plant (see Fig. 4A). The system equations are

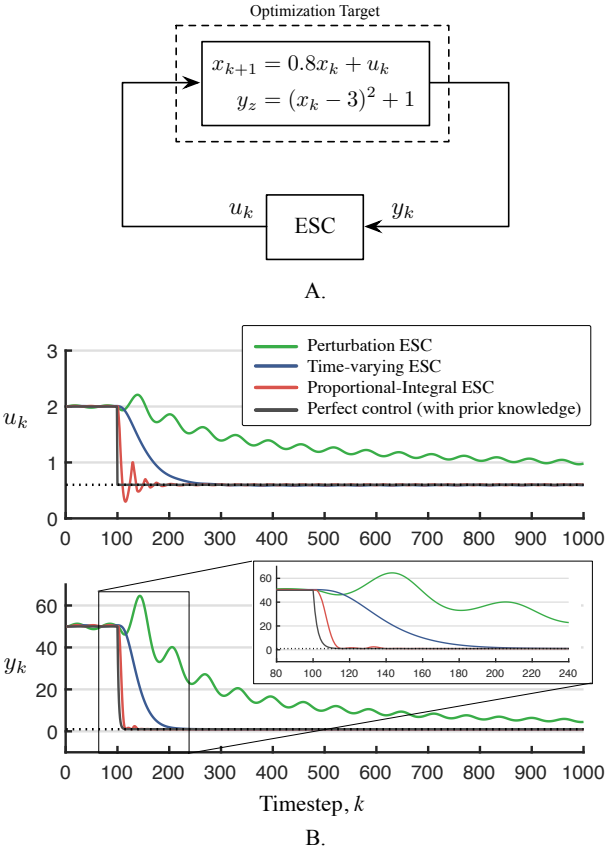

Fig. 4. A. A simple Hammerstein system under extremum seeking control. B. A comparison of the convergence performance of three extremum seeking algorithms. The top plot shows the decision variable u_k and the bottom plot shows the performance metric y_k. The perturbation-based ESC (green) converges to the optimum after about 4000 steps (ultimate convergence not shown for space), Time-varying ESC (blue) converges in about 100 steps, while the PI-ESC (red) converges in about 15 steps—roughly 10 steps longer than the perfect control method (black) which has prior knowledge of the optimizer. The inset figure in the bottom plot shows a detailed view of the convergence.

$$x_{k+1} = 0.8x_k + u_k \quad (17)$$

$$y_k = (x_k - 3)^2 + 1, \quad (18)$$

which has a single optimum point at $u^* = 0.6$, $y^* = 1$.

The pole near the unit circle represents the dominant process dynamics and establishes a fundamental limit on convergence rate. Reasonable effort is made to obtain parameters for all ESC methods that achieve the best possible convergence rates. The perturbation ESC parameters are

$$d_k = 0.2\sin(0.1k)$$
$$\omega_{LP} = 0.03$$
$$K = -0.005$$

Where d_k is the sinusoidal perturbation, ω_{LP} is the cutoff frequency for a first-order low-pass averaging filter, and K is the (integral-action) adaptation gain. A high-pass washout filter is not used as convergence rate is improved without it.

The parameters used for the TV-ESC are

$$d_k = 0.001\sin(0.1k) \qquad k_i = 0.001$$
$$\alpha = 0.1 \qquad \varepsilon = 0.4,$$

where k_i is the (integral-action) adaptation gain, α is the estimator forgetting factor, and ε is the estimator timescale separation parameter.

The parameters used for the PI-ESC are

$$d_k = 0.001\sin(0.2k), \qquad \tau_I = 60$$
$$\alpha = 0.5, \qquad k_g = 0.0003$$
$$K_k = 0.1,$$

where τ_I is the integral time constant, k_g is the proportional gain and is computed from the relationship $k_g = 1/(\tau_I^2)$, α is the estimator forgetting factor, and K_k is the estimation gain. See [18] for detailed parameter definitions.

Simulations are performed starting from an initial input value of $u_0 = 2$ and the ESC methods are turned on after 100 steps. The resulting simulations are shown in Fig. 4B. The perturbation ESC method converges to a neighborhood around the optimum in about 4000 steps (not shown in the figure), the TV-ESC method converges in about 100 steps, while the PI-ESC method converges in about 15 steps. The resulting controller performance is compared to the response obtained from a controller that has *a priori* knowledge of the system optimizer and applied directly in one time step, for which the output settles in about 10 steps. Thus, the PI-ESC approach convergence to the optimizer at the same timescale as the process.

IV. Results

The fast convergence characteristic of PI-ESC is well suited to the optimization of thermal systems with their associated long time constants. In this section, we apply the PI-ESC algorithm to the problem of selecting setpoints for the discharge temperature of a vapor compression system. In the first part, a multiphysics-based model of the vapor compression system is detailed and used to compare TV-ESC and PI-ESC for an initial condition response and disturbance rejection response wherein the boundary conditions are changed. In the second part, experimental work is presented demonstrating convergence on a production-grade room air conditioner.

A. Model Description

A detailed model[1] describing the nonlinear dynamics of the vapor compression cycle is developed using the equation-oriented modeling language Modelica [25]. Physics-based models are constructed for the four principal components shown in Fig. 1A: the evaporating and condensing heat exchangers, the compressor, and the electronic expansion valve. Algebraic models are used for the compressor and the expansion valve because the dynamics of these components are much faster than that of the heat exchangers. The partial differential equations representing the mass, momentum, and energy balances for the refrigerant in the heat exchangers are discretized into 48 volumes along the direction of flow using the 1-D finite volume method. A real gas model of the refrigerant R410A is used for the primary working fluid, and a dry air model is used to describe the changes in the temperature of the secondary working fluid due to heat transfer between the refrigerant and the air through the discretized tube wall. Additional details for this model are found in [26].

[1]We emphasize here that although a brief discussion is offered on model development, the ESC algorithms themselves are not model-based. The model in this section is used as a synthetic plant for controller evaluation and comparison, and does not inform PI-ESC design beyond satisfying the assumptions in Section III-A.

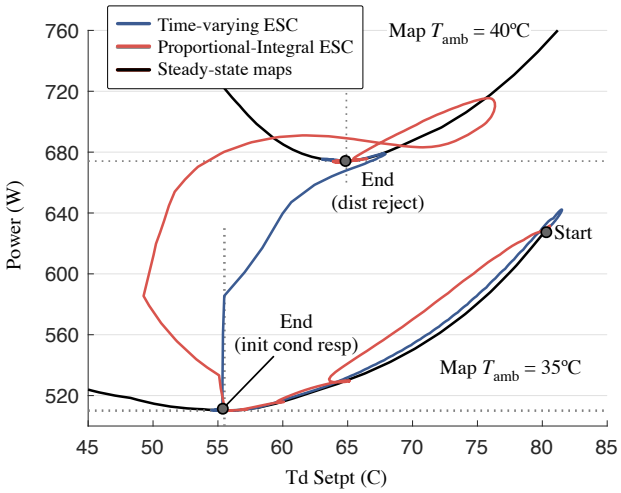

Fig. 5. PI-ESC is compared to TV-ESC using a simulation model of a room air conditioner. Steady state maps are obtained at $35°C$ and $40°C$ (black). The system is initially operated with T_d Setpt $= 81°C$ at $T_{amb} = 35°C$. PI-ESC (red) and TV-ESC (blue) then drive the T_d setpoint such that power is minimized, representing an initial condition response. Next, the ambient conditions are changed to $40°C$ and the ESC methods both converge to the new optimum, rejecting ambient temperature disturbance.

The feedback controller K of Fig. 2 is implemented in Modelica as two PI controllers with the additional dynamic coupling previously described and tuned for disturbance rejection. The PI-ESC algorithm given by Equations (6), (7), (10), (12), (14), (15) and (16) is also implemented in Modelica. Because the PI-ESC algorithm is discrete-time while the model of the vapor compression cycle is continuous-time, the `Modelica.Synchronous` library is used to interface between these two types of system representation using a clocked approach. The resulting cycle and control system comprise a set of 8,663 differential-algebraic equations with 124 state variables, and is compiled and simulated using the Dymola 2016 compiler [27] running on an i7 desktop machine with 8GB of memory.

Using the simulation model, the steady-state map relating power consumption to discharge temperature is obtained at two different ambient temperatures $T_{amb} = \{35°C, 40°C\}$ by slowing sweeping the discharge temperature from $83°C$ to $45°C$ while recording power consumption. The room temperature tracking error and discharge temperature tracking errors are monitored during the sweep to ensure no dynamics are excited. These two maps are convex, as shown in Fig. 5. The convexity can be understood physically as follows: At

the high temperature end of this sweep, the elevated discharge temperatures require relatively little refrigerant returning to the compressor and therefore the compressor discharge temperature feedback loop selects expansion valve commands that are more closed than optimal. As a result, the amount of refrigerant entering the evaporator is restricted, causing a high degree of superheating. As the compressor temperature setpoint is reduced, the feedback loop opens the expansion valve, allowing more refrigerant into the evaporator, which in turn provides more cooling to the zone. As the zone cools below the setpoint temperature, the compressor frequency is reduced by the zone temperature feedback controller, thereby reducing power consumption. This explains the downward slopes in the steady state maps from about 83°C toward the two optimizers.

As the downward ramp continues through the optimum and toward lower T_d setpoints, the power consumption increases. This is explained by the reduction in the system pressure ratio and corresponding loss of cooling capacity caused by opening the expansion valve too much. When the compressor discharge temperature setpoint is set to a value lower than optimum, the expansion valve is opened, causing the evaporating pressure to increase and the condensing pressure to decrease. In order to compensate for the reduced cooling capacity, the zone temperature feedback loop increases the compressor frequency, which in turn increases power consumption at setpoint values lower than the respective map minimizers.

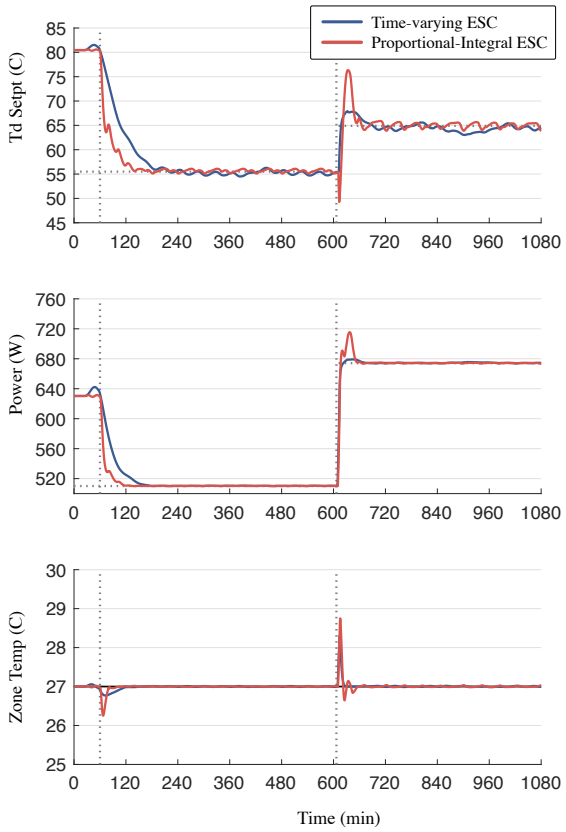

Fig. 6. Extremum seeking decision variable (T_d setpt) and objective (power) as explicit functions of time for TV-ESC (blue) and PI-ESC (red) algorithms. Adaptation is turned on at $t = 60$ min. PI-ESC converges to minimum power in about 60 min. The ambient air temperature is rapidly increased from 35 to 40°C at $t = 610$ min and the new optimal T_d setpoint is discovered on a similar timescale.

B. Simulation results

Simulations are performed comparing TV-ESC to PI-ESC using the model. We initially tried perturbation ESC, but convergence time was similar in scale to the Hammerstein system of Fig. 4 and too long to be practical. Two types of system responses are tested: the ESC algorithms are initialized at a suboptimal operating point and converge to the optimizer under fixed conditions, demonstrating the initial condition response, and a subsequent step change in ambient temperature demonstrates disturbance rejection performance.

In the following simulations, TV-ESC and PI-ESC methods are executed every 60 seconds. The parameters used for the TV-ESC are

$$d_k = 0.5\sin(0.2k) \qquad k_i = 0.02$$
$$\alpha = 0.05 \qquad \varepsilon = 0.9,$$

and the parameters used for the PI-ESC are

$$d_k = 0.5\sin(0.3k), \qquad \tau_I = 1$$
$$\alpha = 0.06, \qquad k_g = 0.5$$
$$K_k = 0.4, \qquad \Theta_k = 50.$$

Initial values for the PI-ESC parameters are obtained using the guidance offered in [19]. We have found it helpful to further refine these parameters in a iterative manner by simulating an approximate model of the optimization target. In this approach, we assume the vapor compression system is a Hammerstein system of the form (17)-(18), with suitable substitutions for a the dominant pole and approximate convex map. While it is generally assumed that the ESC algorithm has no knowledge of the plant, for the practical issue of parameter tuning, approximating the system time constant and steady state map can provide a simple model for ESC parameter tuning, which is further refined on in nonlinear simulations or experiments.

The convergence trajectories are overlaid on the steady state maps and shown in Fig. 5, and the evolution of T_d setpoint, power and zone temperature as explicit functions of time are shown in Fig. 6. T_d setpoint is the ESC decision variable u_k, power is the ESC objective y_k, and the zone temperature T_r is a process variable regulated by the feedback controller K using the compressor. For the first 60 minutes, the dither signal is applied and the estimation equations for each ESC algorithm are turned on, but the adaptation is disabled. This allows the estimator states to settle before control is activated. The adaptation is turned on at $t = 60$ min. Both TV-ESC and PI-ESC converge to the optimal inputs T_d setpoint = 55.5°C, with PI-ESC settling in about 60 min, and TV-ESC settling in about 120 min. The zone temperature initially decreases as the lowered T_d setpoint from $t = 60$ to $t = 180$ introduces more cool refrigerant into the evaporator. The CF is then be reduced

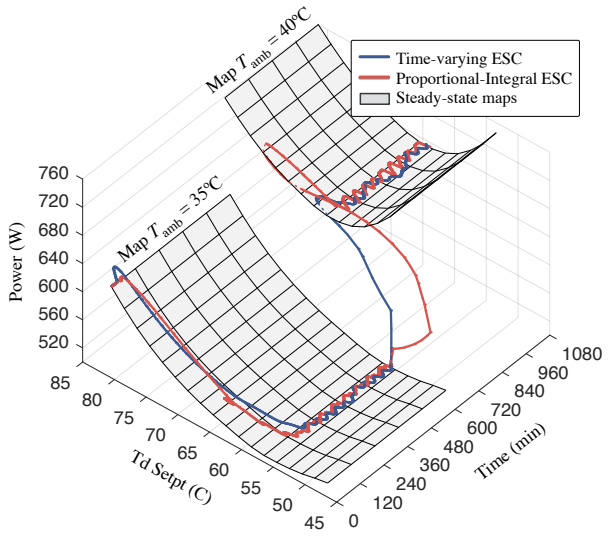

Fig. 7. Evolution of convergence to the map minimizers for TV-ESC and PI-ESC. The values of the T_{amb} disturbance is abruptly changed and the new optimizer is automatically obtained, demonstrating good extremum seeking performance in the presence of high bandwidth disturbances. Figs. 5 and 6 are projections of this data.

by the feedback controller to bring the room temp back up to its setpoint, reducing power consumption.

At $t = 610$ min., the ambient air temperature is rapidly increased (over a five-minute ramp) from 35 to 40°C. Both ESC algorithms converge to the new optimizer on the order of an hour, with PI-ESC exhibiting an overshoot during the transient we attribute to parameter tuning. The zone temperature becomes overheated during the transient, requiring the compressor frequency to increase. The previously discussed feedforward term in K couples the increase in compressor frequency to an increase in T_d setpoint, which improves settling time during this disturbance rejection test. The convergence trajectories toward minimum power are shown as explicit functions of both time and T_d setpoint in Fig. 7. This view illustrates the convex performance map and transient responses of the two ESC methods.

We emphasize that the ambient disturbance is rapidly changed during this simulation with the ESC methods active, and the new optimizer is attained within about 60 min for PI-ESC. During operation of the real system the ambient temperature is expected to vary with a diurnal period of 24 hours, this extremum seeking algorithm has the bandwidth to reject expected T_{amb} disturbances, a capability that has not been previously demonstrated.

C. Experimental Setup

This section describes experiments wherein PI-ESC is used to determine optimal discharge temperature setpoints for a 2.8 kW split-ductless style room air conditioner. The indoor unit (consisting of the evaporating heat exchanger and associated fan) is installed in a 9.8 m^3 adiabatic test chamber, and the outdoor unit (consisting of the compressor, expansion valve, condensing heat exchanger and associated fan) is installed in a 6.2 m^3 adiabatic test chamber. A secondary balance-of-plant system controls the heat load in the indoor unit test chamber and regulates the temperature in the outdoor unit test chamber.

Custom interface electronics are created to enable direct control of the vapor compression system's actuators, and LabVIEW (National Instruments) software collects data from the air conditioner's onboard sensors and additional laboratory instrumentation, and executes the control code for the balance-of-plant system and the vapor compression system under test. The balance-of-plant system is configured to hold the air temperature in the outdoor test chamber to 35°C and the thermal power introduced by electrical resistive heaters in the indoor test chamber to 2100 W for these experiments.

For the subsequent experiments, the air conditioner's production control algorithm is disabled and replaced by a discrete-time feedback controller K regulating zone temperature and discharge temperature as depicted in Fig. 2. The desired zone temperature is set to 26°C, and the compressor discharge temperature setpoint is an experimental variable to be manipulated by either the extremum seeking algorithm, or a slow ramp function to determine the steady state map as described below. The evaporator and condenser fan speeds are held constant.

D. Experimentally-obtained Steady State Map

In order to establish a convex relationship between power consumption and the discharge temperature setpoint, an initial sweep of discharge temperature is performed. The initial discharge temperature setpoint is set to 83°C and the system is operated for two hours in order to reach steady state conditions. The discharge temperature setpoint is subsequently ramped down at a rate of 6°C/hr stopping at a temperature of 40°C. The measured power consumption as a function of the discharge temperature setpoint obtained during this ramp are shown as the gray points of Fig. 8 and the underlying experimentally-obtained map is indeed convex with an optimal discharge temperature setpoint of around 58°C for these conditions.

Note that the experimentally-obtained steady state map of Fig. 8 appears significantly noisier and less smooth than the corresponding signals from the simulations. The reasons are attributed to quantization in both the actuators and sensors described in Sec. II-C which are not included in the simulation model. Additionally, several ranges of compressor frequencies are not accessible by the feedback controller in order to avoid machine resonances or unwanted electrical interactions between the power inverter circuitry and the AC power supply. This accounts for the discrete nature of the steady state map. Within this range, the compressor frequency commands selected by the zone temperature feedback loop alternate between two ends of a large gap in permissible CF commands. Moreover, the sensors used in the feedback loop are also quantized, resulting in 'deadband' areas where the feedback loops cannot obtain zero steady state error and instead cause the process variables to oscillate around their setpoints. This oscillation therefore causes multiple power

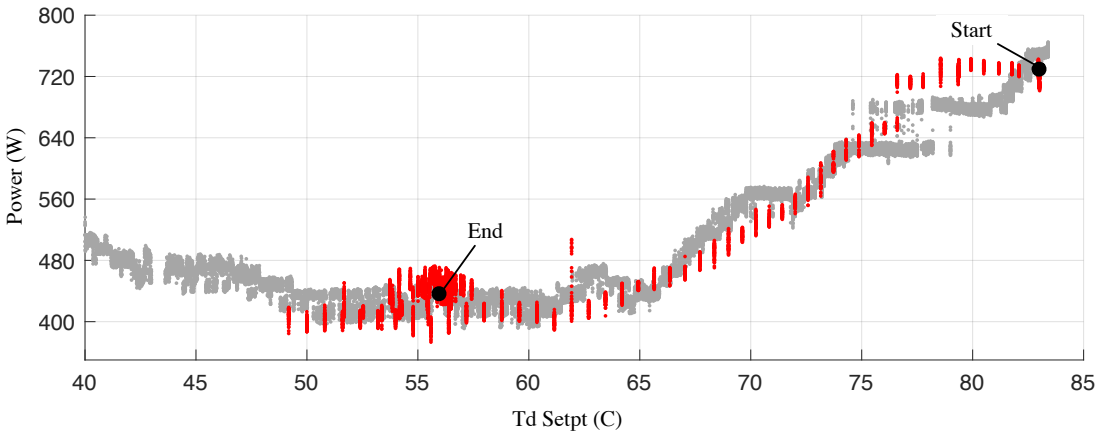

Fig. 8. Experimental data showing PI-ESC convergence on a production-grade room air conditioner. The power-optimal T_d setpoint is automatically discovered by PI-ESC. Discontinuities and discrete-valued setpoints are due to sensor and actuator quantization.

consumption measurements to be obtained for a particular discharge temperature setpoint, explaining the multiple power measurements for a given discharge temperature setpoint—the measured map is not one-to-one due to interactions from the quantization nonlinearities in the feedback loops. Despite this phenomenon, a clear convex trend is observable in this data.

E. Experimental Results

The system is tested under the same thermodynamic conditions used to characterize the steady state map, with the discharge setpoint initially set to $83^{\circ}C$, and the system is allowed to reach steady state under the direction of the PI-ESC algorithm. The PI-ESC selects setpoints for the discharge temperature and is provided with a measurement of the vapor compression machine power consumption. The PI-ESC has no additional information about the location or nature of the optimum setpoint. The parameters used are

$$d_k = 0.05\sin(0.2k), \qquad \tau_I = 0.6$$
$$\alpha = 0.05, \qquad k_g = 1$$
$$K_k = 0.13, \qquad \Theta_k = 10$$

with a sampling period of one minute.

As in the simulations, the estimator part of PI-ESC is turned on and allowed to settle without activating adaptation for the first 10 mins of the transient data shown in Fig. 9. At $t = 10$ min., adaptation is turned on. Discharge setpoints trend toward the optimum and converge after about a 50 min transient. Fig. 9 (top) shows the discharge temperature setpoints selected by the PI-ESC algorithm as well as the discharge temperature controlled by the feedback controller K.

Power consumption (Fig. 9 (middle)) is driven from about 710 W to 440 W, which is a bit higher than the minimum found from the quasi-steady sweep. We note that during the sweep, the feedback controller was disabled, whereas in this experiment it is active and inducing transients in the room temperature (see from Fig. 9 (bottom)) that cause a slightly higher power consumption.

In regions of low compressor setpoint temperatures, two-phase refrigerant may be exiting the evaporator and entering

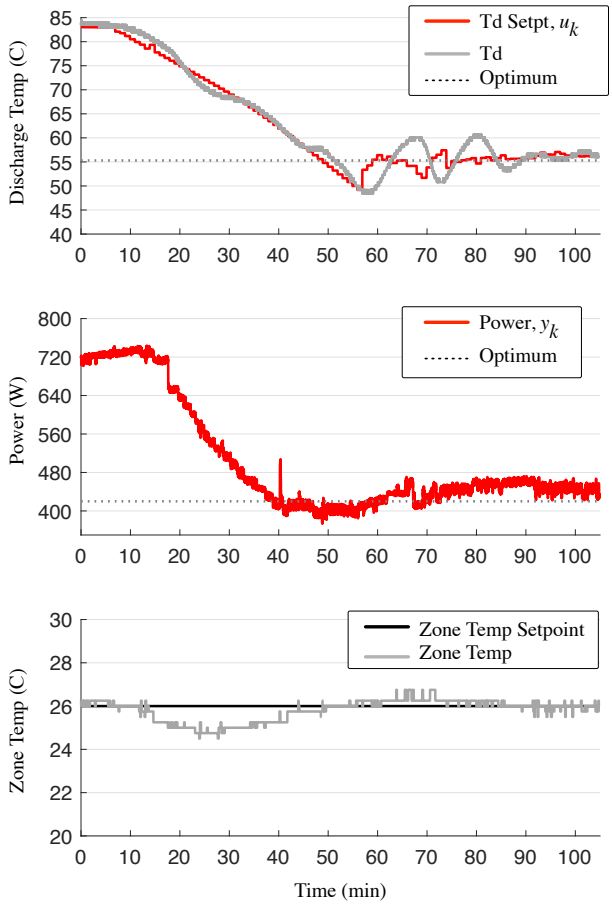

Fig. 9. (top) Time evolution of the discharge temperature setpoint and discharge temperature. Convergence to the optimum occurs in about 60 min. (middle) Power consumption as a function of time is driven toward its minimum. (bottom) Zone temperature is regulated to near its setpoint during the PI-ESC transient.

the compressor, potentially damaging the compressor if this condition is allowed to persist for too long. Consequently, the projection operator parameter Θ_k is selected to limit the rate of change of the setpoint in order to eliminate overshoot that may have caused excessively low setpoint values and potentially damaging liquid refrigerant ingestion. Projecting the estimated parameters $\hat{\theta}$ back into the constraint set therefore serves as an important feature for practical problems where regions of the state space must be avoided for equipment protection. In future work, explicit constraints on the ESC decision variables will be considered, which will require reformulating the estimator for bumpless transition as constraints become active.

V. Conclusion

We have applied a novel proportional-integral extremum seeking algorithm to energy-optimal setpoint selection for a vapor compression system. The rapid convergence properties of the PI-ESC algorithm are especially attractive for vapor compression systems because the relative bandwidths of disturbance rejection of the closed loop system and typical disturbances are such that the system is rarely in equilibrium for periods to satisfy the two timescale separation requirement of traditional perturbation-based ESC. We have demonstrated the improved convergence properties of PI-ESC relative to other methods on an example problem, and used a physics-based model with realistic disturbance properties to show applicability of extremum seeking to vapor compression systems. Finally, we have validated the approach in an experimental scenario where noise and actuator and sensor quantization are significant.

Daniel J. Burns (M'10-SM'18) Daniel Burns received the M.S. and Ph.D. degrees in mechanical engineering from the Massachusetts Institute of Technology, Cambridge, in 2006 and 2010, respectively. Since 2010, he has been with Mitsubishi Electric Research Laboratories (MERL), Cambridge, MA, where he is a Senior Principal Research Scientist. At MERL, Dr. Burns develops and prototypes advanced control methods for vapor compression systems. Before joining MERL, he worked on flight instrumentation and control at the Commercial Aviation Systems division of Honeywell, Inc. (Phoenix, AZ) and NASA's Goddard Space Flight Center (Greenbelt, MD). At MIT, he designed and built mechanisms and controllers for high-speed atomic force microscopes. His research interests include multi-physical modeling and control of mechatronic and thermodynamic systems, instrumentation and experimentation, and applied predictive and adaptive control.

Christopher R. Laughman Chris Laughman is a Senior Principal Research Scientist at Mitsubishi Electric Research Labs investigating the modeling, simulation, control, and optimization of large-scale multiphysical systems. He obtained his Ph.D. in Building Technology at MIT in 2008, and is currently focused on the development of high-performance and energy-efficient building systems.

Martin Guay Martin Guay is a Professor in the Department of Chemical Engineering at Queen's University in Kingston, Ontario, Canada. He received his PhD from Queen's University in 1996. Dr. Guay is Senior Editor for the IEEE CSS Letters. He is deputy Editor-in-Chief of the Journal of Process Control. He is also an associate editor for Automatica, IEEE Transactions on Automatic Control, Canadian Journal of Chemical Engineering and Nonlinear Analysis & Hybrid Systems. He was the recipient of the Syncrude Innovation award and the D.G. Fisher from the Canadian Society of Chemical Engineers. He also received the Premier Research Excellence award. His research interests are in the area of nonlinear control systems including extremum-seeking control, nonlinear model predictive control, adaptive estimation and control, and geometric control.

References

[1] K. J. Chua, S. K. Chou, and W. M. Yang, "Advances in heat pump systems: A review," *Applied Energy*, vol. 87, no. 12, pp. 3611–3624, Dec 2010.

[2] A. Hepbasli and Y. Kalinci, "A review of heat pump water heating systems," *Renewable and Sustainable Energy Reviews*, vol. 13, no. 6–7, pp. 1211 – 1229, 2009.

[3] S. A. Tassou, G. De-Lille, and Y. T. Ge, "Food transport refrigeration—Approaches to reduce energy consumption and environmental impacts of road transport," *Applied Thermal Engineering*, vol. 29, no. 8-9, pp. 1467–1477, Jun 2009.

[4] V. Slesarenko, "Heat pumps as a source of heat energy for desalination of seawater," *Desalination*, vol. 139, no. 1–3, pp. 405 – 410, 2001.

[5] J. Burger, H. Holland, E. Berenschot, J. Seppenwodde, M. ter Brake, H. Gardeniers, and M. Elwenspoek, "169 Kelvin cryogenic microcooler employing a condenser, evaporator, flow restriction and counterflow heat exchangers," in *14th IEEE International Conference On Micro Electro Mechanical Systems*, 2001, pp. 418–421.

[6] R. J. Otten, "Superheat control for air conditioning and refrigeration systems: Simulation and experiments," Master's thesis, University of Illinois at Urbana-Champaign, 2010.

[7] M. S. Elliott and B. P. Rasmussen, "On reducing evaporator superheat nonlinearity with control architecture," *International Journal of Refrigeration*, vol. 33, no. 3, pp. 607–614, 2010.

[8] K. Vinther, H. Rasmussen, R. Izadi-Zamanabadi, and J. Stoustrup, "Single temperature sensor superheat control using a novel maximum slope-seeking method," *International Journal of Refrigeration*, vol. 36, no. 3, pp. 1118–1129, 2013.

[9] D. Burns, W. Weiss, and M. Guay, "Realtime setpoint optimization with time-varying extremum seeking for vapor compression systems," in *American Control Conference*, 2015.

[10] D. Burns and C. Laughman, "Extremum seeking control for energy optimization of vapor compression systems," in *International Refrigeration and Air Conditioning Conference*, 2012.

[11] M. Guay and D. Burns, "A comparison of extremum seeking algorithms applied to vapor compression system optimization," in *American Control Conference*, 2014.

[12] H. Sane, C. Haugstetter, and S. Bortoff, "Building HVAC control systems—role of controls and optimization," in *American Control Conference*, 2006.

[13] P. Li, Y. Li, and J. E. Seem, "Efficient Operation of Air-Side Economizer Using Extremum Seeking Control," *Journal of Dynamic Systems, Measurement, and Control*, vol. 132, no. 3, May 2010.

[14] V. Tyagi, H. Sane, and S. Darbha, "An extremum seeking algorithm for determining the set point temperature for condensed water in a cooling tower," in *American Control Conference*, 2006.

[15] M. Leblanc, "Sur l'*é*lectrification des chemins de fer au moyen de courants alternatifs de fr*é*quence *é*lev*é*e," Revue G*é*n*é*rale de l'Electricit*é*, 1922.

[16] M. Krstic, "Performance Improvement and Limitations in Extremum Seeking Control," *Systems & Control Letters*, vol. 39, no. 5, pp. 313–326, April 2000.

[17] Y. Tan, W. Moase, C. Manzie, D. Nesic and, and I. Mareels, "Extremum seeking from 1922 to 2010," in *29th Chinese Control Conference (CCC)*, 2010.

[18] M. Guay, "A time-varying extremum-seeking control approach for discrete-time systems," *Journal of Process Control*, vol. 24, no. 3, pp. 98 – 112, 2014.

[19] M. Guay and D. J. Burns, "A proportional integral extremum-seeking control approach for discrete-time nonlinear systems," *International Journal of Control*, vol. 90, no. 8, pp. 1543–1554, 2017.
[20] A. Bejan, *Advanced Engineering Thermodynamics*, 3rd ed. Wiley, 2006.
[21] P. Broersen and M. van der Jagt, "Hunting of evaporators controlled by a thermostatic expansion valve," *Journal of Dynamic Systems, Measurement, and Control*, vol. 102, pp. 130–135, 1980.
[22] D. J. Burns, C. Laughman, and S. A. Bortoff, "System and method for controlling vapor compression systems," United States Patent 9,534,820, January 3, 2017.
[23] G. Goodwin and K. Sin, *Adaptive Filtering Prediction and Control*. Dover Publications, Incorporated, 2013.
[24] N. J. Killingsworth and M. Krstic, "PID tuning using extremum seeking: online, model-free performance optimization," *IEEE Control Systems Magazine*, vol. 26, no. 1, pp. 70–79, Feb. 2006.
[25] Modelica Association. (2015) Modelica specification, version 3.3r1. [Online]. Available: www.modelica.org
[26] C. Laughman, H. Qiao, V. Aute, and R. Radermacher, "A comparison of transient heat pump cycle models using alternative flow descriptions," *Science and Technology for the Built Environment*, vol. 21, no. 5, pp. 666–680, 2015.
[27] Dassault Systemes, AB. (2015) Dymola.